scientific reports

Check for updates

OPEN

Loops, topologically associating domains, compartments, and territories are elastic and robust to dramatic nuclear volume swelling

Jacob T. Sanders[1,5], Rosela Golloshi[1,5], Priyojit Das[2], Yang Xu[2], Peyton H. Terry[1], Darrian G. Nash[1], Job Dekker[3,4] & Rachel Patton McCord[1]✉

Layers of genome organization are becoming increasingly better characterized, but less is known about how these structures respond to perturbation or shape changes. Low-salt swelling of isolated chromatin fibers or nuclei has been used for decades to investigate the structural properties of chromatin. But, visible changes in chromatin appearance have not been linked to known building blocks of genome structure or features along the genome sequence. We combine low-salt swelling of isolated nuclei with genome-wide chromosome conformation capture (Hi-C) and imaging approaches to probe the effects of chromatin extension genome-wide. Photoconverted patterns on nuclei during expansion and contraction indicate that global genome structure is preserved after dramatic nuclear volume swelling, suggesting a highly elastic chromosome topology. Hi-C experiments before, during, and after nuclear swelling show changes in average contact probabilities at short length scales, reflecting the extension of the local chromatin fiber. But, surprisingly, during this large increase in nuclear volume, there is a striking maintenance of loops, TADs, active and inactive compartments, and chromosome territories. Subtle differences after expansion are observed, suggesting that the local chromatin state, protein interactions, and location in the nucleus can affect how strongly a given structure is maintained under stress. From these observations, we propose that genome topology is robust to extension of the chromatin fiber and isotropic shape change, and that this elasticity may be beneficial in physiological circumstances of changes in nuclear size and volume.

Imaging and chromosome conformation capture-based approaches have revealed that chromosomes are organized at different length scales into loops, topologically associating domains (TADs), compartments, and chromosome territories[1–3]. Mechanisms such as loop extrusion, phase separation, and tethering of chromatin to nuclear structures are emerging as key players in building and maintaining these chromosome structures[4–9]. However, less is known about the physical properties of these structures and how they respond to perturbation. Are certain features of genome structure held together specifically and robustly while others are weaker or an incidental effect of nuclear crowding? Carefully quantified disruption of isolated nuclei has proven to be a fruitful approach to measure properties of chromosome structures. Fragmenting chromatin inside intact nuclei to varying degrees has revealed the relative stability of different types of chromosome interactions, from strong lamina associations to more dynamic polycomb associated interactions[10]. But, other approaches are needed to measure the elasticity and stability of these interactions in the context of the intact chromosome polymer.

A variety of approaches have been used over the past decades to investigate the physical properties of nuclei and chromosomes, and the results suggest that the 3D genome structure has some elastic properties and some potential for irreversible deformation. When isolated nuclei are stretched by physiological-level forces, the

[1]Department of Biochemistry & Cellular and Molecular Biology, University of Tennessee, Knoxville, TN 37996, USA. [2]UT-ORNL Graduate School of Genome Science and Technology, University of Tennessee, Knoxville, TN, USA. [3]Program in Systems Biology, Department of Biochemistry and Molecular Pharmacology, University of Massachusetts Medical School, Worcester, MA 01605, USA. [4]Howard Hughes Medical Institute, Chevy Chase, MD, USA. [5]These authors contributed equally: Jacob T. Sanders and Rosela Golloshi. ✉email: rmccord@utk.edu

chromatin structure acts like a stretched spring that provides resistance to initial deformations as it stretches, with a spring constant that varies with altered histone modifications and chromatin compaction[11]. Conversely, chromatin also has some properties of a compressed spring. Disrupting interactions between histone tails dramatically releases the energy that is stored in this 'prestressed' compressed state of genome folding, even to the point of exploding the nucleus[12]. Micropipette aspiration experiments have shown that chromatin domains stretch, sometimes irreversibly, as they are pulled into a narrow opening[13]. Microscopic observations have demonstrated visible changes in chromatin structure inside the nucleus after external forces are applied to cells[14,15], and such chromatin deformations can even directly induce gene expression in live cells[16]. In all these experiments, however, chromosomes are typically conceived as coarse-grained objects with uniform physical properties, and there has been little investigation into how specific genomic regions or structures either change or maintain their organization during deformation.

External force exertion on the nucleus likely affects regions of the genome near the applied force disproportionally to the rest of the genome. Thus, localized external nucleus stretching will not allow us to characterize the response of the genome structure to physical perturbation genome-wide in a population of cells. So, in this work, we use low-salt chromatin expansion: rather than pulling on the exterior of the nucleus, salt depletion changes the charge balance along the chromatin, expanding the local chromatin fiber itself, and thus expanding the nucleus from the inside out. This will allow us to monitor the effects on 3D genome topology chromatin fiber extension and nucleus expansion.

Low-salt swelling of isolated chromatin fibers or nuclei has been used for decades to investigate the structural properties of chromatin. Treatment of intact nuclei with EDTA to chelate magnesium ions enabled electron microscopic images of networks of chromatin fibers, but with little ability to interpret the structural patterns observed[17]. Electron microscopic studies of isolated chromatin fibers concluded that removing magnesium and sodium ions from the chromatin causes a state change from a 30 nm fiber to an extended 10 nm fiber[18]. Similarly, isolated mitotic chromosomes undergo reversible decondensation and a decrease in stiffness in low-salt conditions, again, presumably explained by a change from 30 to 10 nm fiber[19]. However, the simple idea of a conversion between a 10 and 30 nm fiber does not explain what would happen to the layers of 3D genome structure in an interphase nucleus during such swelling. In fact, recent work suggests that the 30 nm fiber is uncommon in the in vivo interphase genome structure[20–25], so further work is needed to understand how such in vitro studies translate to the interphase nucleus. Imaging of swollen nuclei after photobleaching has previously suggested that large scale chromatin structures return to their initial positions after swelling and return to the original nucleus size[26]. Meanwhile, experiments with DNA-damaging agents have suggested that notable decondensation of the chromatin occurs during low-salt swelling: chromatin in swollen nuclei is more susceptible to DNA damage by irradiation than high-salt compacted chromatin[27]. So, the question remains, what structures are decondensing during swelling? Is the whole 3D structure really returning to the same state after re-condensation as suggested from whole nucleus observations or are there more subtle effects at a small scale?

In this work, we combine the classic low-salt swelling perturbation approach with detailed measurements of 3D genome interactions using Hi-C. By doing so, we can probe how the layers of genome structure react to or maintain robustness to this physical perturbation. At the same time, similar to expansion microscopy approaches[28], we may be able to detect connections in the structure more clearly by spreading out genomic regions that are not linked by stable interactions.

Results

Chromatin expansion is visibly elastic. To avoid the complicating effects of secondary biological signaling cascades on 3D genome organization, we performed all our experiments with isolated human nuclei. As reported previously[27], we can expand isolated human lymphoblast GM12878 nuclei by replacing a buffer containing physiological levels of cations sodium and magnesium (1×HBSS) with a buffer with no cations and EDTA to chelate any remaining magnesium (Fig. 1A). Expansion happens rapidly (Supplementary Movie 1), indicating that this expansion is a purely physical perturbation, not requiring biologically controlled signals. This initial rapid expansion is followed by a slower further increase in nucleus size over the next 10 min to 1 h (Fig. 1B). When a nucleus is returned to 1×HBSS, it shrinks back to its original size. There is variability in the precise extent of expansion of each nucleus within the population, but all nuclei show at least some expansion, with the average expansion being 2–fivefold in measured cross-sectional area, which corresponds to an estimated 4–tenfold expansion in volume, assuming the nuclei are approximately spherical (Fig. 1B,C). We find that staining chromatin with DAPI causes a measurable shrinking of the expanded nucleus (Supplementary Fig. 1A,B). So, we rely on phase contrast light microscopy to measure the extent of nucleus expansion. However, staining chromatin with DAPI demonstrates that the chromatin fills the entire space of the expanded nucleus (Supplementary Fig. 1A), and it is not the nuclear membrane alone that expands.

We first evaluated the previously reported elasticity of the genome structure by monitoring a photoconverted pattern on nuclei during expansion and re-contraction. Histone H4 fused to photoconvertible Dendra2 was expressed throughout the nucleus and then photoconverted in a specific pattern by 405 nm laser light, prior to expansion. Upon expansion, the fluorophores are spread out such that the pattern is barely visible, but, when the nucleus is recontracted by the replacement of salt, the same pattern that was present before expansion was visible again (Fig. 1D). The photoconverted pattern was also restored upon recontraction in other cell types, and when nuclei were left in the expanded state for an hour (Supplementary Fig. 1C,D) or treated with RNase (Supplementary Fig. 1E).

The visibly apparent elasticity of nucleus expansion is also observed in nuclei with mutant Lamin A and after RNA degradation. Cells expressing progerin, the mutant form of Lamin A that causes Hutchinson-Gilford Progeria Syndrome (HGPS), have stiffer nuclei with characteristic blebs[29,30], and previous work has suggested that

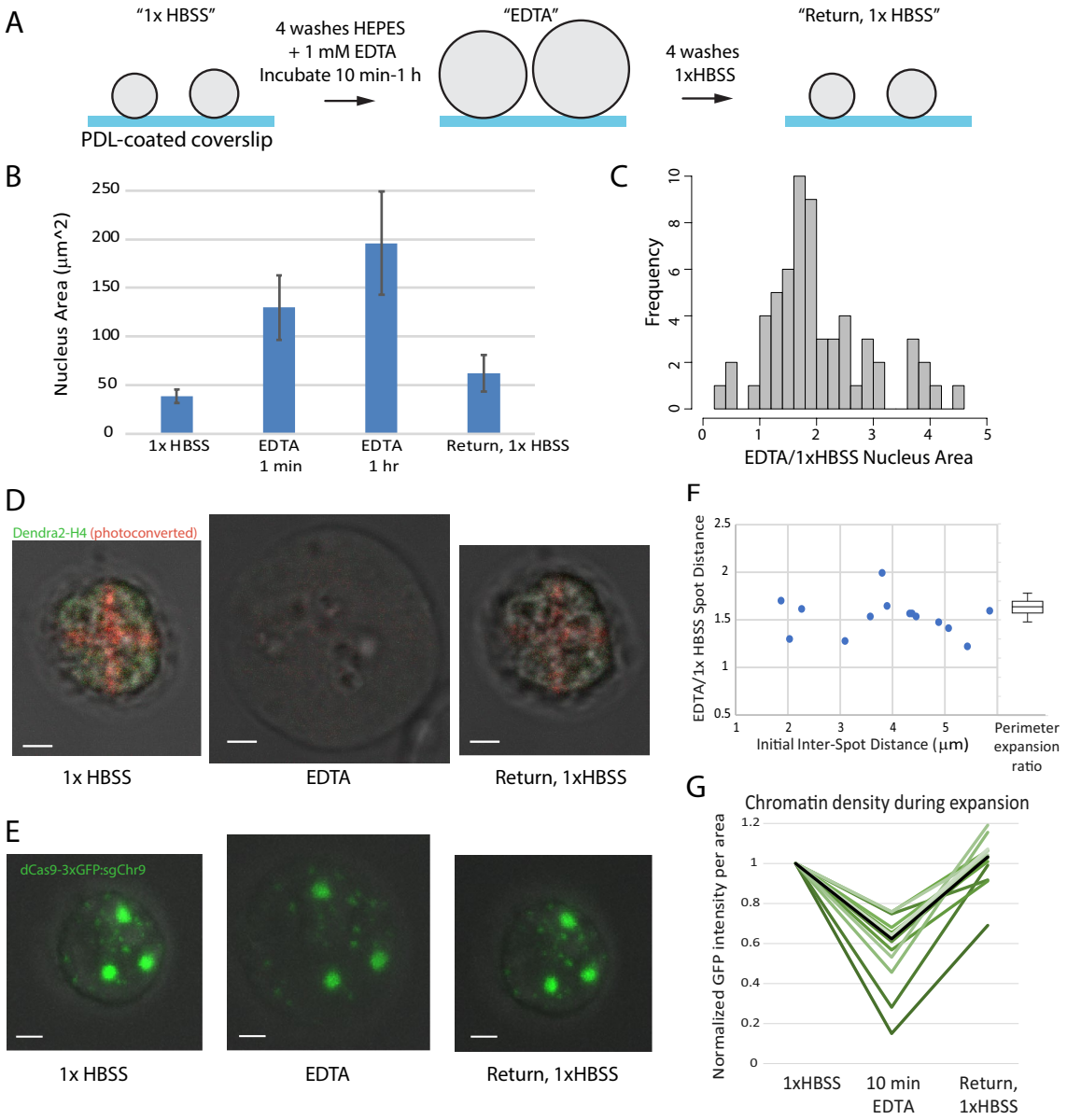

Figure 1. Elasticity of nuclear organization is evident in single cell imaging. (**A**) Experimental design. (**B**) Mean cross-sectional area changes of GM12878 nuclei before, during and after expansion in EDTA (N = 83, 71, 116, 23); error bars = std. dev.) (**C**) Distribution of fold changes in area of individual GM12878 nuclei immediately after EDTA addition (N = 61). Data from one representative biological replicate shown. (**D**) Photoconverted pattern on GM12878 nuclei transfected with Dendra2-H4 is still visible when nuclei are returned to 1× HBSS after expansion in EDTA (scalebar = 2 µm), nucleus treated with RNase prior to experiment. (**E**) CRISPR-dCas9-GFP targeted to chromosome 9 pericentromeric repeats in HEK293T cells. Chromosomes spread out during expansion in EDTA but return to their original locations after return to 1× HBSS. (scalebar = 2 µm). (**F**) The ratio of expanded vs. initial distances between each pair of chromosome 9 spots in HEK293T cells (y axis) is independent of initial distance between spots (Pearson's correlation test not significant: $p = 0.67$) and is comparable to the fold increase in perimeter of these same cells (boxplot, right; Spot distance ratio vs. Perimeter expansion ratio not significantly different, unpaired t-test, $p = 0.1$). (**G**) Quantification of GFP intensity per area during expansion of CRISPR-GFP labeled chromosome 9 repeats in HEK293T cells. Green lines = intensity trajectories of individual chromosome 9 spots; Black line = median of all intensity measurements.

these altered mechanical characteristics make progerin expressing nuclei unable to recontract after expansion[31]. In contrast, we find that fibroblast nuclei stably expressing progerin are able to expand and re-contract (Supplementary Fig. 2A–C). Visible wrinkles in the lamina spread out and become smoother during expansion, but then return to nearly identical positions after contraction. This result also held true when we used transient or stable transfection of progerin in a different cell line (HeLa) (Supplementary Fig. 2D).

Labeling specific loci allows more detailed quantitation of chromosome expansion. These results show a generic elasticity of the genome structure, but do not provide information about the positions of any specific genomic loci. To investigate the effects of expansion on the position of specific chromosomes, we took advantage of the CRISPR imaging system for targeting fluorophores to genomic loci using catalytically inactive Cas9 and sgRNAs complementary to chromosomal repeat regions[32]. Transfection efficiency of these large plasmids was very low in GM12878 cells, so for these experiments, we used U2-OS and HEK293T cells that are easier to transfect. Due to the abnormal karyotype in both of these cell types, 3 fluorescent spots are sometimes observed, representing the pericentromeric regions of 3 copies of chromosome 3 or chromosome 9 in these cells. These pericentromeric chromosome repeat regions spread out from each other proportionally to the swelling of the entire nucleus, and then return to their original positions upon contraction (Fig. 1E,F, Supplementary Fig. 3A).

We further noticed a loss of fluorescence intensity at individual loci in the expanded state, which increased again after re-contraction. After quantifying the fluorescence intensity during expansion for 13 individual loci, we found that all foci decreased in intensity during expansion and recovered during contraction, though with a notable amount of variability in how much each spot increased and decreased. The intensity loss per area is consistent with the cross-sectional area of the chromosome region increasing 1.3–6.6 fold, consistent with the range of increase in size measured for whole nuclei.

The median intensity loss during expansion was 40%, and on average the fluorescence recovered to 100% after re-contraction (Fig. 1G). This change in fluorescence intensity is corrected for the intensity losses caused by repeated imaging, and cannot be explained by a dissociation and re-association of fluorescent proteins, as demonstrated by the lack of any fluorescence recovery after local photobleaching of a labeled locus (Supplementary Fig. 3B). Thus, we conclude that the decreased fluorescence per volume during expansion reflects a local decondensation of the labeled peri-centromeric repeat chromatin region in low-salt conditions. Overall, we can observe that reversible local and global spreading of loci occurs with this expansion.

Hi-C experiments reveal remarkable preservation of genome contacts in expanded nuclei. While microscopy shows quantifiable decondensation and spreading out of labeled genomic loci during expansion, it cannot reveal how specific chromosome structures are affected by this perturbation. To investigate the effect of low-salt nuclear swelling on 3D genome topology and contacts, we performed Hi-C experiments in the 1× HBSS, EDTA, and return to 1× HBSS conditions according to established protocols[33], with modifications necessary to adapt the protocol for adherent isolated nuclei (see "Methods" section). GM12878 nuclei were crosslinked directly on the dishes in which expansion took place, and image quantitation indicates that the expanded size of the nuclei was preserved during this fixation (Supplementary Fig. 3C). The Hi-C protocol utilized was more similar to "dilution" rather than "in situ" Hi-C because nuclei lysis before digestion and ligation was necessary to recover crosslinked chromatin from the poly-D-lysine dishes. As expected, this led to more variable cis/trans ratios among replicate experiments (Supplementary Table 1)[34,35]. In each replicate set, the expanded nuclei EDTA condition was more divergent while 1xHBSS and the return to 1xHBSS conditions were most highly correlated (Supplementary Fig. 4A). We present detailed analyses of the highest quality and most deeply sequenced replicate (EDTA-R1), while checking overall conclusions in the other replicates (Supplementary Fig. 4).

After mapping and correcting the Hi-C data for inherent biases using iterative correction[36], we examined the contact maps at various resolutions, from the whole genome scale down to the level of individual loops. Our results indicate a remarkable preservation of genome structure at all length scales.

At the scale of chromosome territories, Hi-C results indicate that both the enrichment of interactions within individual chromosomes and the patterns of neighboring chromosome arrangements are preserved during nucleus expansion (Fig. 2A,B). The population average evidence for the preservation of chromosome territories through expansion was also validated at the individual nucleus level by multicolor fluorescence in situ hybridization (mFISH) (Supplementary Fig. 3D), though the volume of the expanded nuclei was artificially reduced by the hybridization procedure necessary for FISH. While the size of the nucleus can be preserved during the crosslinking step (Supplementary Fig. 3C), additional ethanol dehydration steps, washes, and denaturation steps can result in some loss of nucleus size, as noted previously[17]. These results indicate that expansion does not cause randomization of chromosome territory locations or significantly more intermingling of chromosomes. The pattern of compartmentalization of genomic regions into the active ("A") and inactive ("B") compartments is also remarkably preserved during expansion, as shown by the highly similar plaid interaction pattern and first principal component of an individual chromosome contact map (Fig. 2C,D, Supplementary Fig. 4B).

At somewhat higher resolution (40 kb bin size), we observe a similar segregation of genomic regions into topologically associating domains (TADs) in both original and expanded conditions (Fig. 3A). The insulation score profile is calculated as previously described using interaction sums within a sliding window along genomic coordinates (see "Methods" section,[37]). Dramatic dips in this profile correspond to TAD boundaries, and the depth of these dips indicates the degree of contact insulation and thus represents the strength of the TAD boundaries. Overall, this insulation profile is highly similar between all three conditions, as can be observed in an example 10 Mb region (Fig. 3A) and quantitatively across whole chromosomes (Fig. 3B, Supplementary Fig. 4C). This suggests that TAD boundaries are preserved during low salt expansion.

Changes in the insulation profile with expansion depend on properties of the chromosome region. Despite the similarities observed above, when TAD insulation profiles were evaluated carefully, we found that different changes were observed depending on the chromatin state and lamin association of the chromosome region. We aggregated insulation scores around all TAD boundaries genome wide that were found

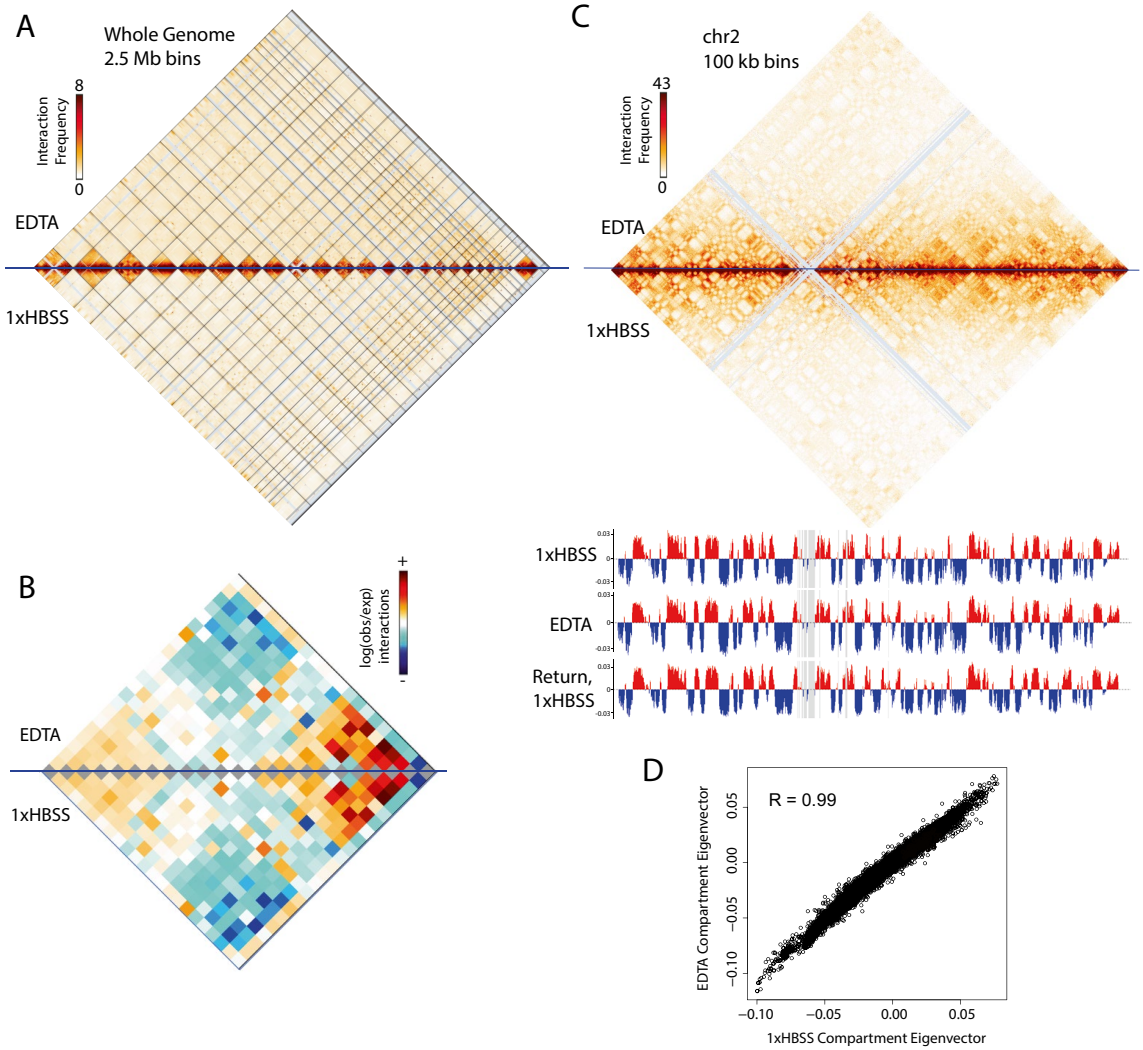

Figure 2. Major features of 3D genome topology are preserved during nuclear expansion. (**A**) Genome-wide contacts from Hi-C performed on GM12878 in EDTA expansion (top) and 1× HBSS (bottom) in 2.5 Mb bins. Black lines = divisions between chromosomes, arranged left to right (chromosomes 1–22, X). (**B**) Observed vs. expected contacts between each pair of chromosomes. (**C**) Contacts within chromosome 2 in 100 kb bins and the first principal component (PC1) below shows little change between A (red) and B (blue) compartmentalization. (**D**) PC1 values are highly correlated between expanded and non-expanded conditions in all 100 kb bins genome wide. All data in this figure from EDTA expansion Hi-C replicate 1. Other replicates shown in Supplementary Fig. 4.

in different subcompartment types[38] and found that while the insulation profiles in A1 (active, early replicating) and B1 (polycomb repressed) regions were unchanged, the entire profile shifted upward in A2 regions and downward in B3 regions (Fig. 3C). Since this insulation score is a sum of contacts within a 160 kb window along the chromosome, this may represent a local increase in contacts in active A2 regions and a decrease in local contacts in B3 regions, which are typically enriched for lamin association. Notably, nucleolus-associated B compartment regions, classified as B4, show an opposite response from other B compartment regions. We confirmed that insulation also varies by lamina associated domain (LAD) type[39], shifting downward (loss of contacts) in regions classified as constitutive LADs (Fig. 3D). The opposing shifts in insulation with expansion in LAD types and subcompartments were reproducible in an independent biological replicate (Supplementary Fig. 4D). To systematically evaluate which chromatin features were associated with these differential changes in insulation profile, we use Ridge and Random Forest regression modeling approaches to identify the relative contributions of chromatin modifications, lamin association and compartment type to the changes we observe at TAD boundaries genome wide (Fig. 3E,F). We found that LaminB and active chromatin marks had opposite weights in the linear model (Fig. 3E), confirming our observation that these region types respond differently to expansion. Since many of these features are correlated (active marks tend to occur in A compartment regions and inactive marks at Lamin associated regions), it is difficult to pinpoint which of these features causes the different local insulation shift with low salt expansion, but it is likely that a combination of lamin association and chromatin state influences how a local region behaves with expansion.

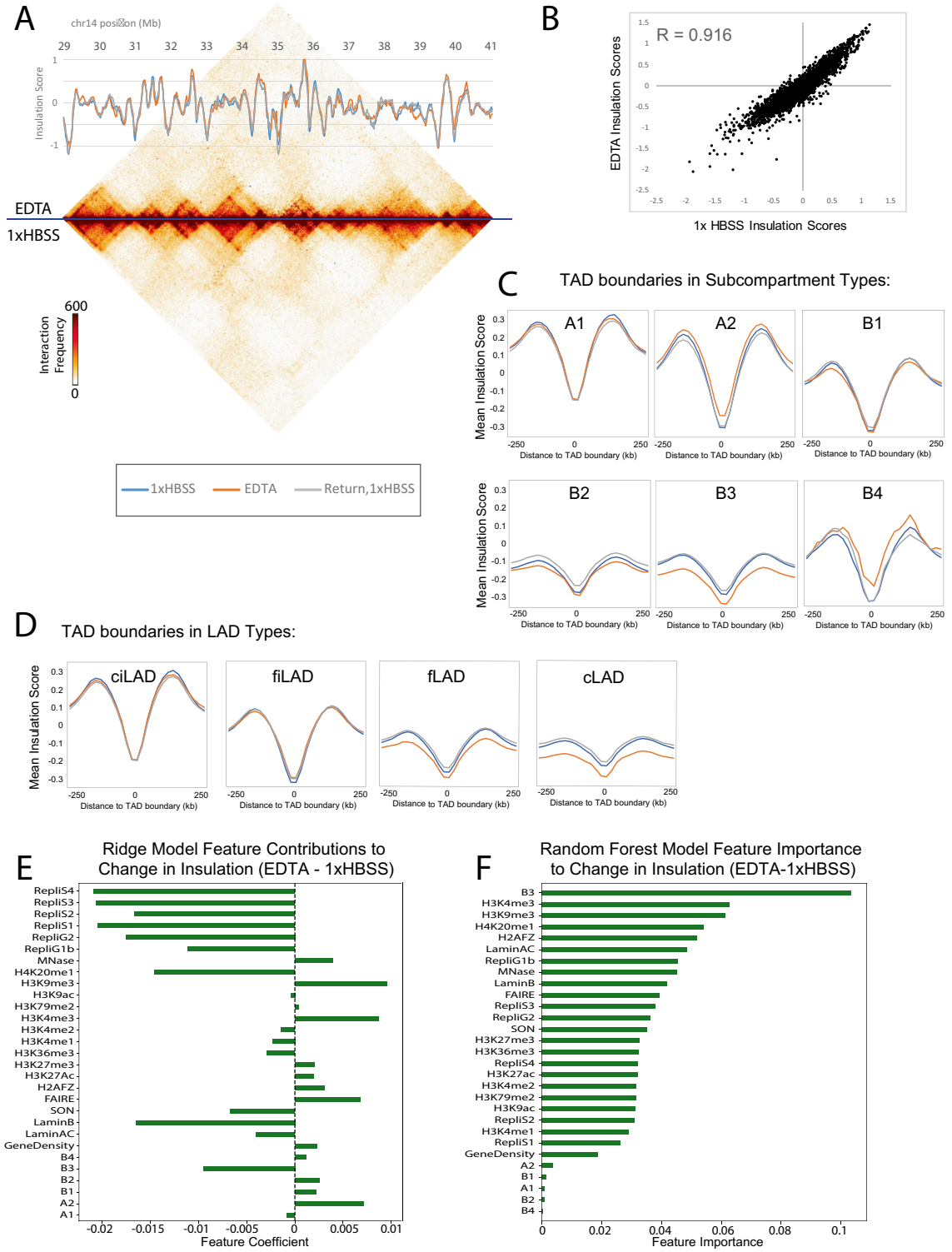

Figure 3. TADs are generally preserved during nuclear expansion. (**A**) Contact map across 12 Mb of chromosome 14 shows the general similarities and minor differences between 1× HBSS (bottom) and EDTA (top). Insulation score (20 kb bin resolution, 160 kb insulation square) is shown overlaid with the heatmap. Throughout the figure blue = 1× HBSS, orange = EDTA, grey = Return, 1× HBSS. (**B**) Insulation scores (calculated same as A) are well correlated (chromosome 2 shown) between expanded and original size nuclei. (**C**) Insulation profiles, calculated as above, are averaged around all TAD boundaries that fall in different subcompartments. (**D**) Averaged insulation profiles across TAD boundaries in different LAD types. (**E**) A ridge regression model was used to fit the change in insulation EDTA—1× HBSS at all TAD boundaries at 100 kb resolution. Coefficients of all factors considered are plotted. (**F**) A random forest regression model was used to evaluate the relative importance of all considered chromatin, lamin association, and subcompartment type features to the difference in insulation between EDTA and 1× HBSS (at 100 kb resolution).

Contact scaling changes reflect elongation of the local chromatin fiber during low-salt expansion. The overall shifts observed in the insulation profile do not indicate a change in TAD boundary strength, but instead suggest an overall change in the local scaling of contacts with distance during expansion. So, next, we turned to examination of this contact scaling. Plotting the average interaction frequency over distance separating two genomic loci can reveal properties of the chromosome fiber[41]. At 40 kb resolution, considering all intrachromosomal interactions across all chromosomes, the scaling plot of interactions over distance shows higher interaction frequency at large genomic distances for both expanded and return to 1× HBSS conditions (Fig. 4A). This suggests that at a large scale, expansion of the chromosomes results in more intermingling of distant chromosome regions, and that some degree of intermingling persists upon return to a normal nucleus size. At smaller distances, a steeper drop in interactions observed in the expanded condition only (Fig. 4B). This measurement captures the extension of the local chromosome fiber previously seen in electron microscopy[18] as the low cation condition alters the charge shielding between nucleosomes. Independent replicates consistently reproduce these key results: the expanded condition shows a steeper drop in interactions at short distances and higher interactions at the longest distances (Supplementary Fig. 4E).

Motivated by the different insulation results observed for different types of chromatin above, we employed a contact-scaling metric that could be evaluated separately at every region across the genome, the distal to local contact ratio (DLR)[42]. DLR quantifies how much each 100 kb genomic bin interacts with distal (greater than 3 Mb away) or local (closer than 3 Mb in linear genomic distance) regions along the chromosome and is similar to the "loss of structure" (LOS) metric used to quantify changes in Hi-C interactions after chromosome fragmentation (Fig. 4C)[10]. The DLR plot in control conditions shows that overall A compartment regions tend to have higher local contacts while B compartment regions have higher distal contacts (Fig. 4C). When we subtract the control DLR from DLR during EDTA expansion, we see that, like insulation, DLR changes differently for different types of chromatin. These different responses may be explained by differences in lamin or nucleolar associations of each chromosome. Genome wide, regions classified as constitutively associated with the nuclear lamina (cLADs)[39] show the strongest increase in distal vs. local interactions during expansion (Fig. 4D, Supplementary Fig. 4F). Further, the LAD-associated B compartment regions (B3) show an opposite DLR change compared to the nucleolus-associated B compartment (B4) regions (Fig. 4E). A linear model evaluating the contributions of different features to this delta DLR shows that LaminB association becomes even more predictive of DLR in EDTA as compared to the control condition (Fig. 4F) and the lamin associated compartment is the most important predictor of the change in distal local ratio overall (Fig. 4G).

Compartment strength weakening and interchromosomal interaction changes with expansion also varies by chromosome. While the A or B compartment assignment of genomic bins across the genome changes very little during expansion, when we examine the strength of interactions within the same compartment type vs. across different compartment types at 100 kb resolution, we do observe a quantitative loss of this compartment strength in the expanded state (Fig. 5A). Interestingly, the loss of compartment strength is most dramatic within the B compartment on small, gene rich interior chromosomes associated with the nucleolus (such as chromosome 19), while the loss of A compartment interactions is more pronounced on chromosomes located near the nuclear lamina, such as chromosomes 2 and 18 (Fig. 5A,B, Supplementary Fig. 4G).

Both chromosomes 17 and 19, which have few LAD domains and instead strong nucleolar associations, show a different pattern of interchromosomal interaction change upon expansion (Fig. 5C). While chromosome 18 shows an increase in its interactions with other chromosomes upon expansion, chromosomes 17 and 19 interact more within themselves and less with other chromosomes after expansion. Thus, chromatin types and LAD status differentially influence changes in contact scaling, the strength of inter-compartmental interactions, and even the interactions between whole chromosomes during low salt expansion.

Effects of expansion on loop extrusion domains. Aggregating the Hi-C interaction signal across previously documented loops in GM12878 cells[38] shows that there is a decrease of loop strength on average during expansion for loops anchored by the insulator protein CTCF (Fig. 6A). However, loops that have neither a CTCF motif nor a measured CTCF peak by ChIP-seq data[43] at either of their anchors do not show a decreased interaction frequency during expansion (Fig. 6B). Factors such as TBP and p300, which have previously been implicated in enhancer promoter looping[44,45], are enriched at loops without CTCF motifs at their anchors (Supplementary Table 2). Taking an aggregate interaction profile of all regions bound by the transcription-associated factor TBP shows a peak of interactions that does not decrease in the way that CTCF-bounded loops decrease during expansion (Fig. 6C). A scatterplot of loop strength relative to local background signal shows that some loops appear to increase in strength while others decrease during EDTA expansion, and then most loops return to their original strength upon return to 1× HBSS (Fig. 6D). When we examined these differential changes in detail, we find several different classes of change that occur in different regions. We observe two categories of loops that decrease in contact frequency with expansion. In one case, we see strong interactions that decrease, while surrounding interaction levels are maintained (Fig. 6E). In the other case, all interactions in a given region decrease uniformly, lessening the apparent loop, and also decreasing interactions within TADs (Fig. 6F). We also observe a set of loops that increase in contact frequency with expansion, becoming more defined relative to the interactions within the TAD that this loop circumscribes (Fig. 6G). In some of these cases, the loop strength is maintained while the "lines" surrounding the strong interaction are decreased (Fig. 6H). These lines have been attributed to the effects of loop extrusion[4], with higher resolution datasets revealing enriched sites of contact along these lines where loop extrusion "pauses" at intermediate CTCF sites and enhancer-promoter interactions[46]. The loss of lines and maintenance of "dots" may indicate that, upon the induced chromatin decompaction, cohesin rings slide until blocked by a CTCF site.

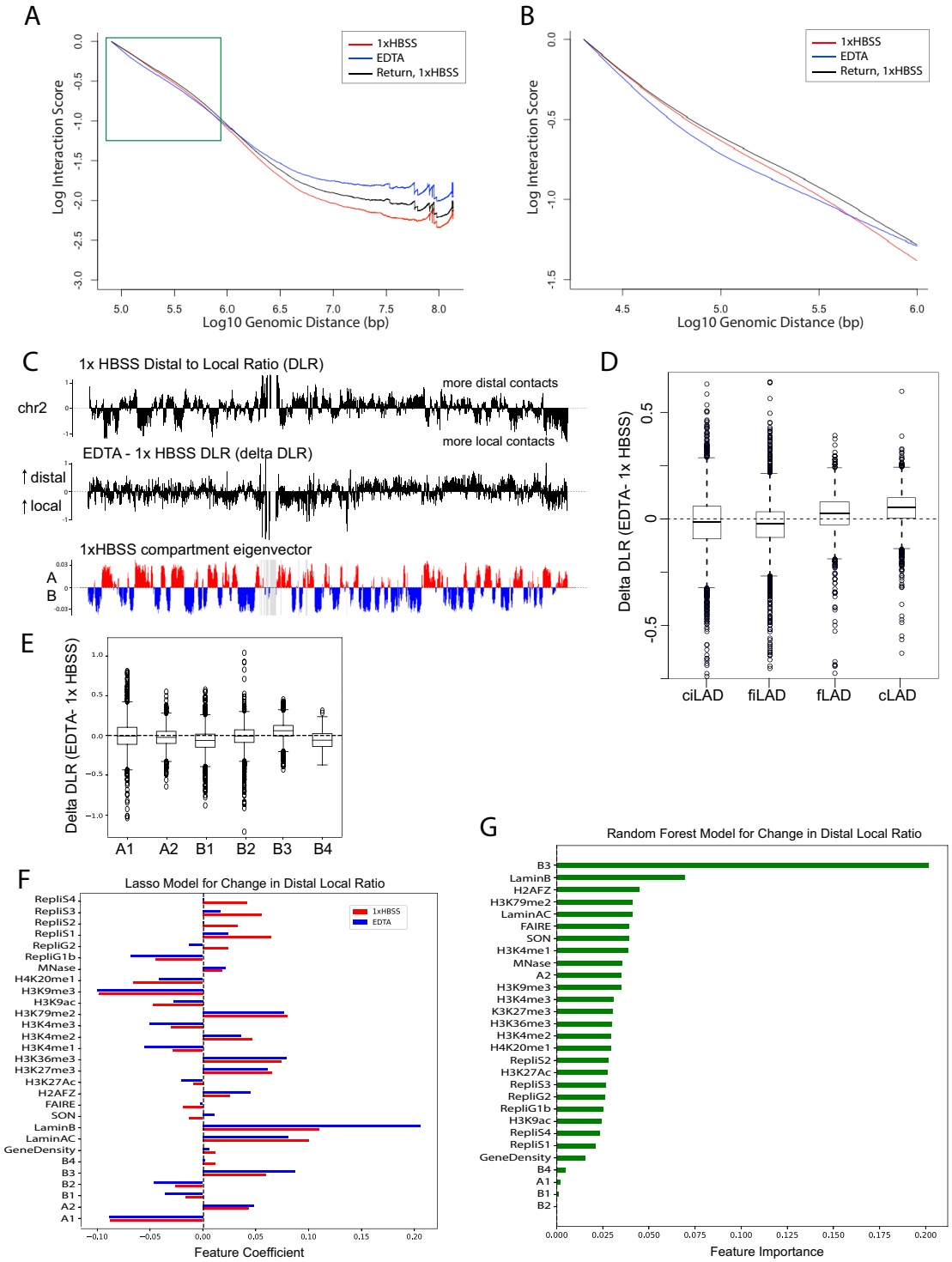

Figure 4. Polymer scaling is altered reflecting chromatin fiber elongation during expansion. (**A**) Log10 interactions vs. Log10 of genomic distance in base pairs for all 40 kb binned intrachromosomal interactions genome wide. A faster drop in local interactions is seen at short distances in EDTA only (green box). (**B**) 10 kb resolution interaction scaling genome wide, zooming in to interactions within 1 Mb. (**C**) The distal to local ratio (DLR) was calculated as the sum of interactions greater than 3 Mb vs. less than 3 Mb for each 100 kb bin (top) and then the difference in DLR was calculated between EDTA and HBSS and median centered (middle). Regions of increased and decreased DLR visually correspond to B and A compartments (bottom). (**D**) Changes in DLR for the whole genome segregated by LAD status as classified by Kind et al.[39] (cLAD = constitutive LAD, fLAD = facultative LAD, fiLAD = facultative interLAD, ciLAD = constitutive interLAD). (**E**) Changes in DLR for the whole genome segregated by subcompartment. (**F**) A ridge regression model was used to fit the DLR for both conditions at 100 kb resolution and the feature coefficients are shown (1xHBSS = red, EDTA = blue). (**G**) A random forest model was used to fit the change in DLR (EDTA—1× HBSS) at 100 kb resolution. Features are sorted by importance.

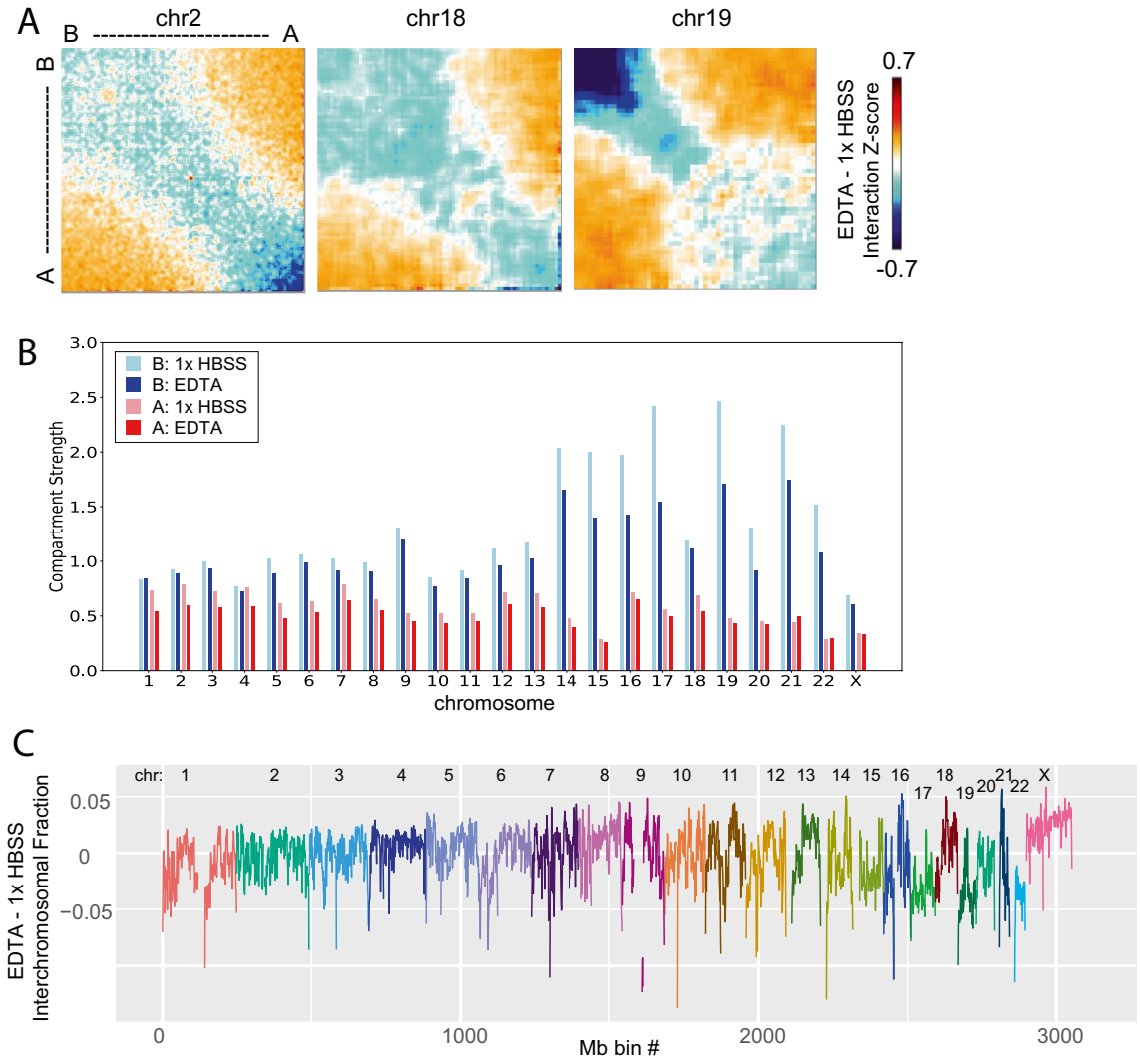

Figure 5. Interaction alterations within the B compartment and lamin associated domains. (**A**) Saddleplots show interaction changes within and between compartments during EDTA expansion. Each matrix is sorted by compartment eigenvector value, from strongest B to strongest A compartment bins. Each pixel represents the difference between interaction Zscore EDTA—1× HBSS. (**B**) The strength of interactions within each compartment (see "Methods" section) calculated for A (pink = 1× HBSS, red = EDTA) and B (light blue = 1× HBSS, dark blue = EDTA) compartments across every chromosome at 100 kb resolution. (**C**) Interchromosomal fraction (trans/cis interactions) difference between EDTA and HBSS is plotted in 1 Mb bins across the genome. Each chromosome is a different color.

The different classes of local interaction change we see do not segregate simply with compartment status or CTCF occupancy. Further investigation will be needed to clarify the different classes of local interaction change that we observe, but we hypothesize that in each case, the more highly reinforced interactions are being preserved during expansion, while contacts that are "transiently or incidentally proximal" are lost. Notably, each of these types of interaction changes are reversible upon return to 1× HBSS, even though the expanded state was maintained for an hour.

Our Hi-C data overall indicates that while many structural features are preserved during expansion, some contacts are lost. To further test this conclusion experimentally, we treated nuclei with increasing concentrations of formaldehyde before expansion. Progressively higher concentrations of formaldehyde rapidly inhibit expansion upon EDTA treatment (Supplementary Fig. 5A). This further suggests that some interactions which are present originally in 1× HBSS (and covalently linked by formaldehyde) must separate in order for full expansion in EDTA to occur.

Nucleus expansion requires initial chromatin compaction and intact chromosome fibers. Our Hi-C results indicate that different chromatin types (A and B compartments and subcompartments) behave differently with expansion. To test the idea that initial chromatin modification state affects nucleus expansion, we treated either intact cells or isolated nuclei with 0.5 μM of the histone deacetylase inhibitor trichostatin A

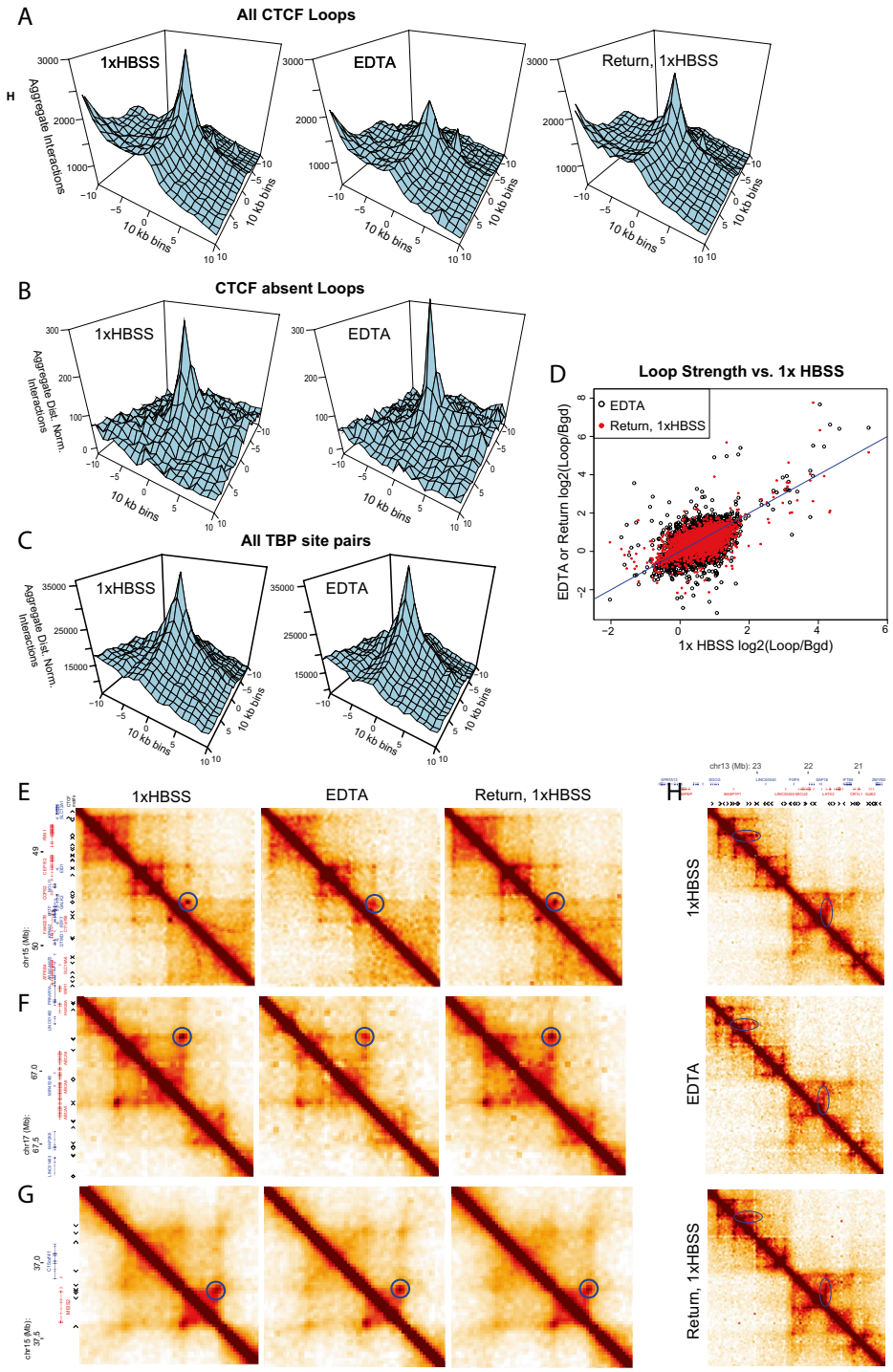

Figure 6. Different categories of loops change differently during expansion. (**A**) Aggregated interactions across all previously annotated loops[38] that contain CTCF sites at both anchors. (**B**) Aggregated log2(observed/expected) distance normalized interactions across all previously annotated loops that have neither CTCF motifs nor ENCODE ChIP-seq CTCF peaks at their loop anchors. (**C**) Aggregated log2(observed/expected) distance normalized interactions for all pairs of TBP binding sites as measured by ENCODE in GM12878. (**D**) Each point represents the log ratio of interactions in the 30 kb bin containing the loop vs. the interactions in a donut around this loop (bgd). Red points represent loop strength upon return to 1×HBSS vs. the original 1×HBSS strength while black points represent EDTA loop strength. (**E**–**H**) Variations in loop strength during expansion in different regions. Each plot is binned at 20 kb, smoothed to 40 kb. Gene positions and CTCF motif positions shown at left. Areas of change highlighted in blue circles in 1×HBSS plot (**E**, **F**) Decreased interactions. (**G**) Increased interaction. (**H**) Loss of loop extrusion lines during expansion.

(TSA) for either 2 or 24 h. This treatment has been widely used for its ability to increase histone acetylation and decompact chromatin[47,48], and has been shown to make nuclei less stiff and more able to be stretched by external forces[49]. Even in isolated nuclei, real time chromatin modification changes have been seen upon treatment with histone deacetylase inhibitors[50]. In isolated nuclei, antibody staining for histone modifications can be performed without crosslinking[50], allowing us to monitor the same stained nucleus across expansion conditions. TSA treated nuclei showed very little expansion upon buffer switch into EDTA (Fig. 7A–C). This result coincides with the previously suggested idea of the pre-stressed state of the nucleus[26], which springs outward upon salt change. Once TSA treatment has already altered this pre-stressed state by decondensing the chromatin, little further expansion is possible in low salt conditions. Interestingly, TSA treated nuclei never reach the size of low salt expanded nuclei (Fig. 7B), suggesting that increased acetylation decondenses the genome in a way that allows more intermingling of chromatin domains, reducing the polymer persistence length, and thus the chromosomes exert less force on the nucleus exterior than low salt expansion with maintained chromosome topology.

We further find that digesting DNA inside isolated nuclei with an endonuclease[10] also inhibits nucleus low salt expansion (Fig. 7D). Moderate digestion with a 6-cutter enzyme tempers the nucleus swelling somewhat, while digestion with a more frequently cutting 4-cutter enzyme effectively prevents nucleus expansion. Previous results show that this degree of 6-cutter digestion cuts the genome into 10–15 kb fragments, but that the genome structure is still held together by relatively many stable associations at this level of digestion[10]. Our expansion results suggest that with an intact fiber, or at least a sufficient degree of maintained associations (mild digestion), the expansion of the fiber causes the whole structure to be forced outward. However, under conditions of digestion which reduce the spring constant and stiffness of the nucleus[10], the pre-stressed state of the chromatin structure is lost and overall nucleus expansion does not occur. It may be that with this further fragmentation, local domains can expand and intermingle with each other without exerting force on the entire nucleus.

Imaging stained chromatin in expanded nuclei reveals additional chromatin structure detail. We observed that 3D genome contacts are largely preserved in the expanded nucleus, while average distances between genomic regions increase. Thus, we predicted that imaging expanded nuclei labeled for certain chromatin types or regions should provide visually more distinct chromatin structure information. Combining this idea with the fact that fluorescent immunostaining of histone modifications can be performed without fixation in isolated nuclei[50], we stained isolated GM12878 nuclei for H3K9Ac, a mark of active chromatin. Before expansion, the staining pattern fills large regions of the nucleus in a diffuse and overlapping pattern (Supplementary Fig. 5B). But, after 10 min of low salt expansion, the intensity of the H3K9Ac staining decreases as the chromatin spreads out (Supplementary Fig. 5C, Supplementary Movie 1) and a larger number of distinct puncta becomes visible (Supplementary Fig. 5D). The original staining pattern is restored upon re-contraction, confirming again that structures were not dramatically broken or rearranged during expansion (Supplementary Fig. 5B).

Discussion

Overall, our results reveal both the overall robustness of the 3D genome structure to low salt nucleus swelling and demonstrate the utility of this expansion approach to reveal differences in the properties of different types of chromosome interactions. Nucleus expansion and re-contraction does not lead to major systematic rearrangements in compartment identity, chromosome positions, TAD boundary positions or loops. The reversibility of the expansion condition that is observed microscopically is borne out at the level of chromosome contacts as well. Interestingly, this result coincides with the computational predictions obtained from polymer physics models. Polymer models have predicted that local changes at the scale of unfolding the 30 nm fiber would not affect the larger scale conformations of the chromosome[51]. These results suggest that fundamental properties of the genome structure allow local chromatin unfolding without dramatic disruption of larger scale chromosome organization.

We observe changes in the local decay of interactions with genomic distance upon expansion, and while these changes create a notable overall shift in TAD insulation profiles, TAD boundary positions are maintained. This suggests that genome topology can be largely independent of chromosome compaction. Indeed, genome topology may be tuned to facilitate robustness to nuclear shape change. The elastic expansion observed in normal nuclei can be destroyed either by strengthening connections through mild crosslinking or by removing connections by causing DNA breaks. This suggests that the genome topology maintains a level of connectivity that promotes both the elasticity and robustness of the resulting structure. Such a pre-stressed spring state may be key to the support of the physical structure of the nucleus by the 3D chromatin folding[49,52]. Strikingly, the weakening of connections, particularly B compartment interactions, that we do observe during EDTA induced expansion are similar to the loss of B compartment interactions observed after cells have deformed their nucleus to squeeze through tight constrictions[53,54]. This suggests that there may be shared features of chromosome structure change during nucleus deformation in general.

These findings also have implications for biological circumstances in which visible expansion and contraction of nuclei are observed. Here, we have used changes in cation concentration as an artificial perturbation to examine chromosome structural properties, but such cation changes can also happen in vivo. Chromosome compaction upon ATP depletion and expansion upon return to normal ATP levels has been shown to depend on changes in cation and polyamine concentrations[55,56]. Often, when these large visible changes in the size of the nucleus are observed in vivo, it is assumed that the topology of genome contacts must be fundamentally rearranging. Our results would suggest that such changes might actually be accommodated without causing substantial rewiring of genome contacts. On the other hand, future work is needed to determine whether the subtle changes we observe in contact frequencies at certain loops and within TAD substructures could in fact have important biological outcomes, even while so much of the genome organization is unchanged. It is also

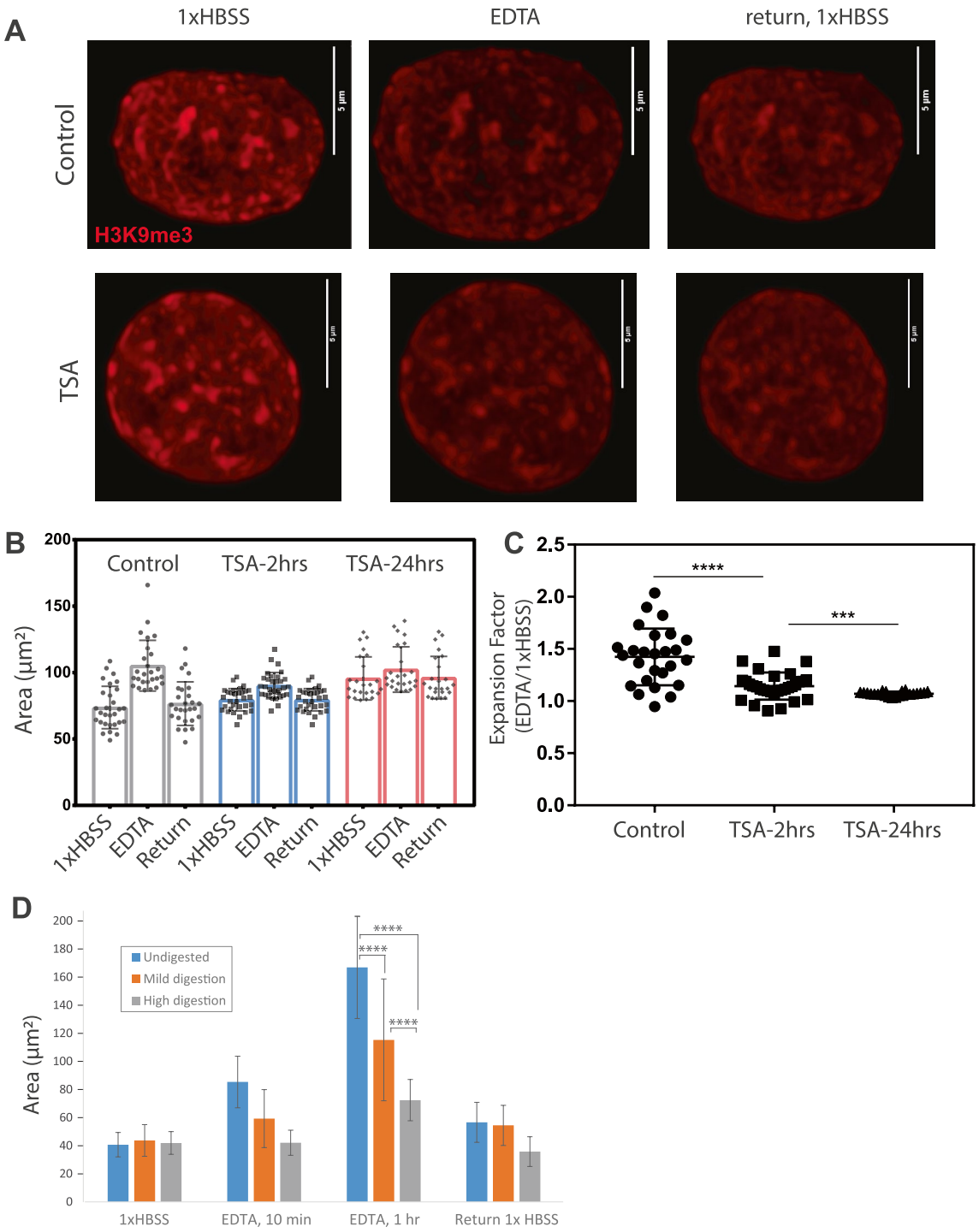

Figure 7. Expansion inhibited by pre-treatment with chromatin decondensing or DNA digesting agents. (**A**) Isolated A375 cell nuclei were treated with TSA for 2 or 24 h, stained without crosslinking with H3K9me3, and then expanded with EDTA for 10 min. Images show maximum projection of a confocal Z stack; scale = 5 µm. (**B**) Area of each nucleus in each condition. One biological replicate shown. Median +/− std dev with full range of data shown as points. (**C**) Expansion factor = (EDTA/1× HBSS nucleus area) for each nucleus analyzed (N = 29, 32, and 24 respectively) ***$p = 0.0005$, ****$p < 0.0001$, Wilcoxon Mann Whitney test). (**D**) Isolated nuclei with no treatment, mild digestion (HindIII for 4 h, 37 °C) or high digestion (DpnII for 4 h, 37 °C) before expansion. Significant differences detected between degree of expansion between each different digestion condition (****$p < 0.0001$, ANOVA and Tukey's multiple comparisons test).

important to note that our observations of the robustness of 3D genome contacts during low salt expansion are true on average across the population of nuclei. However, even when the mean structure does not change, there may be increased variation around the mean during low salt expansion across individual single cells. Future work with single cell Hi-C experiments and chromosome fluctuation analyses[57] will be necessary to clarify this point.

Beyond relevance to physiological circumstances, our results provide another tool to perturb the nucleus and observe physical aspects of the genome structure. These results can be incorporated into future models that aim to explain chromosome structure, such as the loop extrusion model of TAD formation. It is particularly striking that CTCF loops, even though somewhat weakened during expansion, are overall preserved or restored upon return to original salt conditions. Our results also provide a baseline for future work using expansion to perturb and assay effects on the chromosome structure. Future work will be needed to determine whether the subtle changes in structures we observe at 1 h of expansion would become exacerbated by additional time in this expanded state. Starting from our observations of the overall robustness of genome structures to expansion, future work, some of which is already underway[58], is also needed to define what architectural proteins and other factors are key to maintain this structure under expansion stress.

Finally, our results reveal subtle, but consistent differences in how different regions of the genome respond to expansion. We consistently observe different contact frequency changes between peripheral, lamin associated, heterochromatin regions and internal, euchromatic or nucleolus associated regions. These categories of chromosome regions are differently affected by expansion in their local scaling changes, TAD insulation profile changes, compartment strength, and inter- vs. intra-chromosomal interaction frequencies. More work will be needed to determine how much these differences are dependent on physical tethering to structures like the lamina and nucleolus and whether they relate to local histone modification differences. It may be that lamin associations hold more distal regions of chromosomes together during the general spreading of expansion, while the more distal interactions of interior regions are not tethered, and thus are lost during expansion. Alternatively, nucleolus association could influence the degree to which different chromosomes expand and spread during expansion. Pointing to the potential importance of local chromatin state, we observe that global histone acetylation increases decrease the propensity of the nucleus to expand at all in low salt. This result is in line with our observations that it is the B compartment (inherently lower histone acetylation to begin with) that decreases interactions more with expansion than the A compartment (which has a higher initial acetylation state). Further, we observe that different types of looping interactions respond differently to expansion. Future work is needed to clarify whether these different classes of loops are formed by different processes and what factors contribute to their different properties.

Methods

Cell lines. GM12878 cells were acquired under a Material Transfer Agreement from the Coriell Institute and were cultured in RPMI with 15% FBS. U2-OS, HEK293T, IMR90, B16-F1, and A375 cells were acquired from ATCC and cultured as recommended.

Plasmid constructs. The Dendra2-Histone H4 plasmid was derived in part from a photoactivatable GFP-Histone H4 plasmid that was a kind gift of Dr. Roeland Dirks. The H4 gene was isolated from this plasmid by PCR using primers containing KpnI and BamHI sites:

5′ end of Histone H4 + KpnI: 5′-GCGCGCGGTACCATGTCTGGTAGAGGCAAAGG-3′

3′ end of Histone H4 + BamHI: 5′-GCGGATCCCGGGTCAGCCACCAAAGCCGTACA-3′.

Histone H4 was then cloned into the multiple cloning site of the pDendra2-C vector (Clontech catalog# 632546). The dCas9-3xGFP and C3-sgRNA and C9-sgRNA plasmid for CRISPR imaging were a kind gift of Dr. Hanhui Ma and Dr. Thoru Pederson. The GM12878 cells were transfected with pDendra2-H4 using Kit L and program Y-001 on a Lonza Nucleofector IIb. B16-F1 cells were transfected with pDendra2-H4 using the Attractene Fast-Forward protocol (Qiagen). U2-OS and HEK293T cells were transfected with dCas9-3xGFP and C3-sgRNA or C9-sgRNA plasmid at a 1:10 ratio using Lipofectamine 3000 (Thermo Fisher).

To carry out expansion experiments on progerin expressing nuclei, IMR90 cells were retrovirally transduced to stably express either wildtype LaminA (pBABE-puro-GFP-wt-lamin A; Addgene Plasmid #17662) or progerin (pBABE-puro-GFP-progerin; Addgene Plasmid #17663). The plasmid was packaged and delivered using the Phoenix-AMPHO (ATCC® CRL-3213) system. After GFP expression was observed (~2 days), nuclei were isolated and expansion experiments carried out as described below. HeLa cells were transduced to stably express progerin using the same approach above. For transient progerin expression, HeLa cells were transfected with 1 µg of pEGFP-Δ50 LMNA (Addgene Plasmid #17653).

Nuclei isolation. GM12878 nuclei were isolated with the following approach. 1×10^8 cells were collected by centrifugation ($200 \times g$, 5 min, room temperature) and then washed twice with 10 mL ice-cold 1× dPBS and then twice with 5 mL ice cold Nuclei Buffer (NB) (10 mM PIPES pH 7.4, 2 mM $MgCl_2$, 10 mM KCl, 1 mM DTT, H_2O pH 7.4) containing protease inhibitors (Thermo Scientific). After final wash and spin, the cell pellet was resuspended in 10 mL NB + 0.06% NP-40, vortexed gently, and then allowed to equilibrate on ice for 10 min. Cells were then homogenized on ice using a Dounce homogenizer (Pestle A) with 10 slow strokes, rest for 20 min on ice, then 10 more strokes if needed. The cells were examined under a microscope after each 10 strokes to evaluate the degree of lysis and nucleus release. Cells may lyse with 10–30 strokes. To remove excess cellular material, 5 mL of lysed cell mixture was layered on top of a 20 mL sucrose cushion: 30% sucrose in NB and centrifuged for 10 min at $730 \times g$. The supernatant and interface was carefully removed and the pellet containing nuclei was resuspended in either 1× Hank's Balanced Salt Solution (HBSS: 1.26 mM $CaCl_2$, 0.49 mM $MgCl_2$, 0.41 mM $MgSO_4$, 5 mM KCl, 0.44 mM KH_2PO_4, 4.17 mM $NaHCO_3$, 137.9 mM NaCl, 0.34 mM Na_2HPO_4, 5.56 mM

D-Glucose) for immediate use, or in Nuclei Storage Buffer pH 7.4 (10 mM PIPES pH 7.4, 20 mM NaCl, 80 mM KCl, 50% glycerol, 250 mM sucrose, 0.5 mM DTT, 1× protease inhibitors) for storage at − 80 °C for later use.

U2-OS, HEK293T, A375, IMR90, and B16-F1 nuclei were isolated using the same method as previously described after detaching cells with trypsin. Adherent cell types typically required more Dounce homogenization strokes than suspension cells.

Expansion and contraction conditions. Isolated nuclei in 1× HBSS were plated onto 35 mm poly-D-lysine coated glass bottom dishes (MatTek P35GC-1.5-10-C) for imaging or poly-D-lysine coated 100 mm culture plates for Hi-C experiments (Corning BioCoat 356469), and maintained at 4 °C for a few hours or overnight until nuclei were settled and adhering to the dish. Nuclei must be adhered to a surface so that buffers can be fully exchanged without exerting centrifugation forces on the nuclei. Expanded nuclei are fragile and often rupture with centrifugation. Nuclei were expanded by removing 1xHBSS carefully with a pipette until only a thin layer of liquid remained (complete drying would destroy nuclei) and washing nuclei with 1 mM EDTA in 10 mM HEPES buffer pH 7.4 three times. Imaging occurred immediately upon addition of EDTA and in time intervals ranging from 10 min to an hour. In one set of experiments (including pDendra labeled nucleus expansion in Fig. 1), 25 µg RNAse in 200 µL 1× HBSS was added to nuclei for 10 min before EDTA expansion was carried out. We found no detectable effect of this RNAse treatment either on the photoconverted pattern or the expansion properties. All other experiments shown were performed without RNAse.

For expansion experiments on cells pre-treated with TSA for 2 h, A375 cells were treated with 0.5 µM Trichostatin A (TSA—Millipore Sigma T1952) for 2 h before nuclei isolation. After the incubation, A375 nuclei were isolated as previously described with addition of 0.5 µM TSA for each nuclei isolation buffer. Then, isolated nuclei were settled into the PDL coated dish and expansion was carried out as usual (1× HBSS, then 10 min EDTA and then 10 min recovery in 1× HBSS). For 24 h TSA treatment, isolated nuclei from A375 control cells were settled on 35-mm dishes overnight. They were then exposed to 0.5 µM TSA for 24 h. After exposure to TSA, nuclei were expanded with EDTA/HEPES as described above.

Hi-C experiments were performed after 1 h of EDTA expansion. Nuclei were returned to their contracted pre-EDTA state by removing EDTA and washing with 1× HBSS three times. The contracted state was then imaged immediately afterward and in time intervals ranging from 10 min to an hour. Hi-C experiments were performed 20 min after return to 1× HBSS. One Hi-C replicate was performed with expansion performed as above, but replacing 1× HBSS with 0.1× HBSS instead of HEPES-EDTA.

Antibodies and isolated nucleus staining. To stain isolated nuclei for heterochromatin marks, nuclei were settled in a PDL coated dish in 1× HBSS and then stained with a protocol adapted from[50]. Specifically, nuclei were incubated for 1 h in a solution containing 5% FBS and 1:500 primary antibody (H3K9me3; Abcam ab176916 or H3K9Ac; Abcam ab32129) in 1× PBS. The nuclei were then washed twice with PBS 5% FBS and then incubated with secondary antibodies (Fisher Goat anti-Rabbit Secondary Antibody Alexa 488 or Alexa Fluor 594; R37116 or R37117) in PBS 5% FBS for 1 h. Finally, the nuclei were washed twice with PBS 5% FBS. Stained nuclei could then be treated with EDTA for expansion.

Imaging and image analysis. Changes in nucleus size with expansion were quantified by taking images at 40× magnification on an EVOS FL (Thermo Fisher) microscope. Expansion was typically performed on the microscope stage so that the same nuclei could be captured before, during, and after expansion. Nucleus dimensions were quantified using ImageJ by manually fitting an ellipse around each nucleus.

Patterns were drawn on pDendra2-H4 expressing GM12878 nuclei typically using 6–10 scans of 4–5% power of a 405 nm laser on a Leica Confocal SP8 microscope. CRISPR-GFP images were collected at the same intensity of a 488 nm laser for all conditions, and a stack of images from the top to the bottom of each nucleus was acquired. The intensity of fluorescent foci was quantified in ImageJ using the maximum projection image. The average of 3 background measurements were subtracted from the mean fluorescence across each spot area. All measurements were expressed as a fraction of the initial intensity of the spot in the 1× HBSS condition and then normalized by the average intensity loss of spots that were not expanded, but only imaged 3 times in the 1xHBSS buffer (to account for the mild photobleaching after taking multiple stacks of images).

Progerin-expressing, H3K9me3 stained and TSA-treated A375 expansion images were acquired using the Leica SP8 confocal microscope.

To quantify the intensity of H3K9Ac staining before, during, and after expansion, nuclei were manually fitted with an ellipse in ImageJ and the mean gray value intensity was calculated for each ellipse. To quantify the number of detectable H3K9Ac puncta, first, each image was converted to 8 bit and thresholded so that the top 10% of pixels remained. Then, the ImageJ function Analyze Particles was used to determine the number of discrete separate regions of H3K9Ac using a minimum particle size of 15 pixels.

mFISH. mFISH using human chromosome-specific probes were performed as recommended by the manufacturer (MetaSystems,70 Bridge St., Suite 100, Newton, MA 02458 USA) and in previous studies[59]. Briefly, isolated GM12878 nuclei were settled and allowed to attach in 1xHBSS in 8-well chamber slides (MatTek CCS-8). After settling, 4 of the chambers were washed gently 3 times with 200 µl HEPES 1 mM EDTA and allowed to expand for 1 h at 4 °C. Two of these chambers were then returned to the original salt conditions with 3 washes of 1× HBSS. All chambers were then fixed for 10 min in a solution of 2% formaldehyde in the corresponding buffer (1× HBSS or HEPES/EDTA). After crosslinking was stopped with glycine, the chambers were washed once with their corresponding buffer (HBSS or HEPES/EDTA) and then dehydrated by incubating for 2 min each in 70% and absolute ethanol. Chambers were removed and slides were then stored at − 20 °C until mFISH processing.

For mFISH, slides were rehydrated in a series of 1 min ethanol washes: 100%, 70%, 50%, and 30%. After washes with 0.1× (1 min) and 2xSSC (30 min, 70 °C), slides were denatured in 0.07 N NaOH at room temperature, 1 min. Slides were then washed with 0.1× SSC, 4 °C, 1 min and 2xSSC, 4 °C, 1 min and then dehydrated in graded series of ethanol (30%, 70%, 90%, and 100%) and air dried. The mFISH probes were denatured separately by incubation at 75 °C for 5 min followed by incubation at 37 °C for 30 min to allow the annealing of repetitive DNA sequences. An aliquot of the 10 mL probe was placed on the slide and covered with a coverslip. The slides were kept in a humidified hybridization chamber at 37 °C for at least 72 h. The unbound probe was removed by washing the slides in prewarmed (75 °C) SSC (pH 7.0–7.5) for 5 min followed by incubation in 4xSSCT (4xSSC with0.1% Tween 20) for 5 min. Images of interphase nuclei and metaphase chromosomes were acquired using a Metasystems Metafer Platform with a Zeiss epifluorescence microscope equipped with a 63× objective and five optical filters for the excitation of five different fluorochromes [FITC, Spectrum Orange, Texas Red, DEAC, and Cy5]. Territories specific for each homologous pair of chromosomes were identified by unique chromosome-specific processed color generated by the Isis software (MetaSystems). For acquisition, a single two-dimensional image was captured using multiple filters.

Digestion and crosslinking before expansion. To test the effect of intact vs. fragmented chromosomes on expansion, isolated nuclei were, subjected to either 50 U HindIII per µg of DNA (mild digestion) or 10 U DpnII per µg of DNA (high digestion). Nuclei were allowed to settle on a PDL coated coverslip dish and then the density of nuclei per area was estimated under a 40× objective. The amount of DNA in each coverslip dish was estimated as (# nuclei/mm^2) × (314 mm^2/dish) × (6.2×10^{-6} µg DNA/nucleus). This DNA quantity was used to calculate the amount of restriction enzyme to use. Nuclei were incubated with restriction enzyme in 1× CutSmart buffer (New England Biolabs) for 4 h at 37 °C and then washed with 1xHBSS before expansion.

To test the effect of formaldehyde crosslinking on nucleus expansion, nuclei were settled in PDL coated coverslip dishes and then crosslinked with either 0.25%, 0.5%, 1%, 2%, or 5% formaldehyde in 1× HBSS for 10 min at room temperature. Crosslinking was quenched with glycine and then dishes were washed with 1× HBSS before expansion experiments.

Hi-C. Hi-C experiments were performed essentially as described previously, but with a few important modifications. 10–20 million cells were used for each condition. Crosslinking was performed with 1% formaldehyde pre-mixed with the corresponding appropriate buffer (1× HBSS, or 1 mM EDTA + 10 mM HEPES) immediately before addition to the plates of nuclei. After 10 min, crosslinking was quenched with glycine, and plates of crosslinked nuclei were washed in the same buffer corresponding to their expansion or contraction condition. It was not possible to harvest and collect nuclei by scraping and centrifugation due to the fragility of the nuclei, particularly in the expanded case, so nuclei were lysed directly in plates by aspirating all liquid and then adding 1.8 mL of 0.3% SDS in 1× NEB2 buffer (New England Biolabs) per 10 cm dish. Dishes were incubated with gentle agitation at 37 °C for 30 min. Crosslinked material was then removed the plate by scraping. If more than one plate was to be combined to obtain enough cells, the SDS-cell mixture scraped from the first plate was transferred to the second plate for another round of incubation, so that cells from all plates were combined into a final volume of less than 3 mL. SDS was sequestered by addition of 1.8% Triton (final concentration). Crosslinked complexes were then divided into aliquots of 560 uL each to match other Hi-C protocols, and were then subjected to digestion with HindIII overnight (500 U per 560 uL aliquot), biotin fill-in, and dilute ligation as previously described[33].

Hi-C sequencing and contact matrix construction. Hi-C libraries were sequenced on an Illumina GAIIx, HiSeq, or NovaSeq platform with paired end reads. Sequencing reads were mapped to the human genome (hg19), filtered, and iteratively corrected as previously described[36] (https://github.com/dekkerlab/cMapping). For library quality and mapping statistics see Supplementary Table 1.

Hi-C reproducibility assessment. A Spearman correlation-based metric was used to assess reproducibility across all Hi-C datasets, as previously described in Sanders et al.[60] After taking the log of iteratively corrected 1 Mb binned interaction counts and excluding the diagonal bin, correlation maps were calculated for each individual matrix. Each entry in such a Hi-C data correlation matrix represents the correlation between the full row and column of data at that position in the matrix across the entire genome. These individual condition correlation matrices were then used as input to the calculation of pairwise correlations between datasets.

Interchromosomal interaction analysis. The relative frequencies of interactions between each chromosome was determined by comparing the observed number of Hi-C reads involving interactions between two chromosomes to the number of interactions expected to occur between them according to the total numbers of reads observed on each chromosome. This calculation was performed using the equation previously described[61] using the collapseMatrix.pl script available at https://github.com/dekkerlab/cworld-dekker.

Compartment analysis and compartment strength saddle plots. Compartment analysis was performed by running principal component analysis using the matrix2compartment.pl script from https://github.com/dekkerlab/cworld-dekker. Since the PC1 sign (positive or negative) is arbitrary, A compartment identity was assigned to whichever group of bins had the higher gene density. The PC1 value was then used to determine compartment identity for 100 and 250 Kb binned matrices. Saddle plots were constructed to investigate changes in interaction frequency between or within compartments Interaction zScores, normalizing for interac-

tion decay with genomic distance, were calculated according to the matrix2compartment.pl at 250 kb bin size. Then Zscore matrices were reordered based on compartment strength (from strongest B to strongest A using PC1 values). The control condition was subtracted from the expanded condition and then the final matrices were smoothed at a 500 Kb bin size.

To calculate A-A and B-B compartment interaction strengths for each chromosome, distance corrected Hi-C intra-chromosomal interaction frequencies at 250-kb resolution were reordered according to their corresponding PC1 values (from strongest B to strongest A). Then, the reordered intra-chromosomal interaction matrix was smoothed at 500-kb resolution. Interactions were classified as A-A, B-B, and A-B and thresholded to include only the top 20% of interactions. The median value of each A-A, B-B, and A-B interaction was calculated. Finally, the A-B median interaction was subtracted from either A-A or B-B interaction median.

Insulation score and TAD analysis. Topologically associating domain (TAD) boundaries were called using the InsulationScore method[37], available as matrix2insulation in the cworld-dekker github package. The insulation score was calculated at two different resolutions: 20 kb matrix bin size with a 160 kb insulation square size (the distance within which interactions would be summed) and 40 kb bin size with a 520 kb insulation square size. The matrix2insulation script then calls TAD boundaries as minima in the insulation score profile.

To calculate the average insulation score profile around sets of TAD boundaries, the computeMatrix and plotProfile tools were used from deepTools2[62] as implemented in Galaxy Version 3.3.2.0.0 https://usegalaxy.org/. Sets of boundaries that occur in certain compartments or LAD types were identified with the bedtools intersect function[63]. Subcompartment classifications of regions were used as previously calculated for GM12878 cells, downloaded from https://www.ncbi.nlm.nih.gov/geo/query/acc.cgi?acc=GSM1551550[38].

Interaction scaling with distance analysis. Using 40 and 10 kb binned iteratively corrected and scaled contact matrices, we extracted contact frequencies between bins at each genomic distance, excluding the diagonal bin (zero distance). A loess fit was then used to find a smooth curve describing interaction decay vs. distance (using the matrix2loess.pl script in cworld-dekker). The interaction frequencies were then normalized to set the maximum value (loess fit interaction value for the minimum distance) for each dataset to 1 and then plotted on a log scale vs. log genomic distance. For 10 kb bin size, the maximum distance considered between two loci was capped at 1 Mb.

Distal local ratio and interchromosomal fraction. The ratio of interchromosomal interactions relative to the total number of interactions for a given chromosome was calculated as previously described[42]

$$ICF = \frac{Interchromosomal\ Interactions}{Inter + Intra\ chromosomal\ Interactions}$$

$$deltaICF = ICFBottom - ICFTop$$

The log2 ratio of Hi-C interactions with distance greater than 3 Mb relative to local interactions less than 3 Mb away was defined as the Distal to Local Ratio. To find the change in DLR after expansion, delta DLR was calculated as $DLR_{EDTA} - DLR_{HBSS}$ as previously described[42].

$$DLR = log2\frac{Distal\ Interactions\ (> 3\,Mb)}{Local\ Interactions\ (< 3\,Mb)}$$

Ridge and random forest modeling of insulation and DLR changes. In order to examine the contribution of different genomic properties to the insulation or DLR profile at a genome-wide scale, a total of 24 genomic properties were used as predictors (or features) in regression models (Supplementary Table 3). For all the predictors and the response variable, the genome-wide data is binned at 100 kb resolution. Among all these features, the subcompartment profile is the only categorical one and has a total 6 categories (A1, A2, B1, B2, B3 and B4). Therefore, we use a one-hot encoding technique to represent each of these separately and end up with a total of 29 features. We then apply standard scaler normalization technique to each of the features to center them around 0 and scale by the standard deviation. For both the Ridge and Random Forest regression, 'scikit-learn' python package is used. Default parameters are used for training in each model. In one case, the difference between DLR (EDTA-1xHBSS) was used as the response variable and in the other case the difference in the 20 kb bin, 160 kb step insulation score difference, averaged across each 100 kb bin was used for the response variable.

Looping interaction analysis. For analysis of changes in looping interactions, we began with the set of loops previously defined from deeply sequenced GM12878 Hi-C data[38]. We then classified these loops as CTCF containing loops if the loop anchor sites contained CTCF motifs on both sides according to the information in the Rao et al. supplementary table.

Factors enriched at loop anchors (Supplementary Table 2) were found as follows. ENCODE transcription factor binding site data was obtained for GM12878 as a set of narrowPeak files available in the UCSC genome table browser for hg19[43]. Each loop anchor site was screened for overlap with these transcription factor peaks. Then the fraction of anchors occupied by a given factor was compared with the average overlap of the same factor with randomly selected sets of the same number of genomic regions.

To count a loop as a non-CTCF loop, we first applied the criteria that neither loop anchor have a CTCF motif annotated in the Rao et al. data[38]. We found that this initial "non-CTCF" loop set was still quite enriched for CTCF ENCODE peaks (Supplementary Table 2). Therefore, we further excluded all loops where either loop anchor overlapped with a CTCF peak from the following ENCODE datasets: wgEncodeAwgTfbsBroadGm12878CtcfUniPk.narrowPeak, wgEncodeAwgTfbsSydhGm12878Ctcfsc15914c20UniPk.narrowPeak, wgEncodeAwgTfbsUtaGm12878CtcfUniPk.narrowPeak, and wgEncodeAwgTfbsUwGm12878CtcfUniPk.narrowPeak.

TBP site interactions were defined as follows. First, genomic locations binding Tbp in GM12878 cells were assigned according to ENCODE data set wgEncodeAwgTfbsSydhGm12878TbpIggmusUniPk.narrowPeak[43] made available in the UCSC Genome Table Browser (http://genome.ucsc.edu/cgi-bin/hgTables) for hg19. Then, all possible combinations of Tbp binding sites separated by more than 50 kb were considered as potential looping interactions.

For a given set of interactions, the aggregate interactions were calculated as follows: Hi-C data, binned and corrected at 10 kb resolution for each condition and the corresponding looping interaction list was input into the interactionPileUp.pl script from cworld-dekker. This script extracts interaction sub-matrices 100 kb upstream and downstream of each loop anchor pair and then sums all interactions across all sub-matrices. We then further summed pile up matrices across all chromosomes to produce the final aggregated interaction plots.

To define the strength of each loop for plotting and comparing between conditions, we again used the set of loops defined by Rao et al. and 10 kb binned Hi-C matrices for each condition. At each loop position, we calculated the ratio of the interactions in the loop bin divided by the sum of interactions of the bins surrounding the loop.

Data availability

All raw and processed Hi-C data files are available on GEO, accession number GSE182665.

Received: 1 September 2021; Accepted: 9 March 2022
Published online: 18 March 2022

References

1. Dekker, J. & Mirny, L. The 3D genome as moderator of chromosomal communication. *Cell* **164**, 1110–1121. https://doi.org/10.1016/j.cell.2016.02.007 (2016).
2. Gibcus, J. H. & Dekker, J. The hierarchy of the 3D genome. *Mol. Cell* **49**, 773–782. https://doi.org/10.1016/j.molcel.2013.02.011 (2013).
3. McCord, R. P., Kaplan, N. & Giorgetti, L. Chromosome conformation capture and beyond: Toward an integrative view of chromosome structure and function. *Mol. Cell* **77**, 688–708. https://doi.org/10.1016/j.molcel.2019.12.021 (2020).
4. Fudenberg, G. *et al.* Formation of chromosomal domains by loop extrusion. *Cell Rep.* **15**, 2038–2049. https://doi.org/10.1016/j.celrep.2016.04.085 (2016).
5. Nuebler, J., Fudenberg, G., Imakaev, M., Abdennur, N. & Mirny, L. A. Chromatin organization by an interplay of loop extrusion and compartmental segregation. *Proc. Natl. Acad. Sci.* **115**, E6697–E6706. https://doi.org/10.1073/pnas.1717730115 (2018).
6. van Steensel, B. & Belmont, A. S. Lamina-associated domains: Links with chromosome architecture, heterochromatin, and gene repression. *Cell* **169**, 780–791. https://doi.org/10.1016/j.cell.2017.04.022 (2017).
7. Ganji, M. *et al.* Real-time imaging of DNA loop extrusion by condensin. *Science* **360**, 102–105. https://doi.org/10.1126/science.aar7831 (2018).
8. Strom, A. R. *et al.* Phase separation drives heterochromatin domain formation. *Nature* **547**, 241–245. https://doi.org/10.1038/nature22989 (2017).
9. Golfier, S., Quail, T., Kimura, H. & Brugués, J. Cohesin and condensin extrude DNA loops in a cell cycle-dependent manner. *Elife* **9**, e53885. https://doi.org/10.7554/eLife.53885 (2020).
10. Belaghzal, H. *et al.* Liquid chromatin Hi-C characterizes compartment-dependent chromatin interaction dynamics. *Nat. Genet.* **53**, 367–378. https://doi.org/10.1038/s41588-021-00784-4 (2021).
11. Stephens, A. D., Banigan, E. J., Adam, S. A., Goldman, R. D. & Marko, J. F. Chromatin and lamin A determine two different mechanical response regimes of the cell nucleus. *Mol. Biol. Cell* **28**, 1984–1996. https://doi.org/10.1091/mbc.E16-09-0653 (2017).
12. Mazumder, A., Roopa, T., Basu, A., Mahadevan, L. & Shivashankar, G. V. Dynamics of chromatin decondensation reveals the structural integrity of a mechanically prestressed nucleus. *Biophys. J* . **95**, 3028–3035. https://doi.org/10.1529/biophysj.108.132274 (2008).
13. Irianto, J., Xia, Y., Pfeifer, C. R., Greenberg, R. A. & Discher, D. E. As a nucleus enters a small pore, chromatin stretches and maintains integrity, even with DNA breaks. *Biophys. J.* **112**, 446–449. https://doi.org/10.1016/j.bpj.2016.09.047 (2017).
14. Maniotis, A. J., Chen, C. S. & Ingber, D. E. Demonstration of mechanical connections between integrins, cytoskeletal filaments, and nucleoplasm that stabilize nuclear structure. *Proc. Natl. Acad. Sci. U S A* **94**, 849–854 (1997).
15. Guilak, F. Compression-induced changes in the shape and volume of the chondrocyte nucleus. *J. Biomech.* **28**, 1529–1541 (1995).
16. Tajik, A. *et al.* Transcription upregulation via force-induced direct stretching of chromatin. *Nat. Mater.* **15**, 1287–1296. https://doi.org/10.1038/nmat4729 (2016).
17. Woods, P. S., Ledbetter, M. C. & Tempel, N. Preservation of EDTA-expanded grid-mounted chromosomes and nuclei for electron microscopy using a specially designed freeze-dryer. *J. Electron Microsc. Tech.* **18**, 183–191. https://doi.org/10.1002/jemt.1060180214 (1991).
18. Widom, J. Physicochemical studies of the folding of the 100 Å nucleosome filament into the 300 Å filament. *J. Mol. Biol.* **190**, 411–424. https://doi.org/10.1016/0022-2836(86)90012-4 (1986).
19. Poirier, M. G., Monhait, T. & Marko, J. F. Reversible hypercondensation and decondensation of mitotic chromosomes studied using combined chemical-micromechanical techniques. *J. Cell Biochem.* **85**, 422–434 (2002).
20. Razin, S. V. & Gavrilov, A. A. Chromatin without the 30-nm fiber: Constrained disorder instead of hierarchical folding. *Epigenetics* **9**, 653–657. https://doi.org/10.4161/epi.28297 (2014).
21. Maeshima, K., Ide, S., Hibino, K. & Sasai, M. Liquid-like behavior of chromatin. *Curr. Opin. Genet. Dev.* **37**, 36–45. https://doi.org/10.1016/j.gde.2015.11.006 (2016).
22. Krietenstein, N. & Rando, O. J. Mesoscale organization of the chromatin fiber. *Curr. Opin. Genet. Dev.* **61**, 32–36. https://doi.org/10.1016/j.gde.2020.02.022 (2020).
23. Ou, H. D. *et al.* ChromEMT: Visualizing 3D chromatin structure and compaction in interphase and mitotic cells. *Science* **357**, eaag0025. https://doi.org/10.1126/science.aag0025 (2017).

24. Maeshima, K., Ide, S. & Babokhov, M. Dynamic chromatin organization without the 30-nm fiber. *Curr. Opin. Cell Biol.* **58**, 95–104. https://doi.org/10.1016/j.ceb.2019.02.003 (2019).
25. Dekker, J. Mapping in vivo chromatin interactions in yeast suggests an extended chromatin fiber with regional variation in compaction. *J. Biol. Chem.* **283**, 34532–34540. https://doi.org/10.1074/jbc.M806479200 (2008).
26. Mazumder, A. *et al.* Prestressed nuclear organization in living cells. *Methods Cell Biol.* **98**, 221–239. https://doi.org/10.1016/S0091-679X(10)98010-2 (2010).
27. Takata, H. *et al.* Chromatin compaction protects genomic DNA from radiation damage. *PLoS ONE* **8**, e75622. https://doi.org/10.1371/journal.pone.0075622 (2013).
28. Chen, F., Tillberg, P. W. & Boyden, E. S. Expansion microscopy. *Science* https://doi.org/10.1126/science.1260088 (2015).
29. Ribeiro, A. J., Khanna, P., Sukumar, A., Dong, C. & Dahl, K. N. Nuclear stiffening inhibits migration of invasive melanoma cells. *Cell Mol. Bioeng.* **7**, 544–551. https://doi.org/10.1007/s12195-014-0358-3 (2014).
30. Shumaker, D. K. *et al.* Mutant nuclear lamin A leads to progressive alterations of epigenetic control in premature aging. *Proc. Natl. Acad. Sci. U S A* **103**, 8703–8708. https://doi.org/10.1073/pnas.0602569103 (2006).
31. Dahl, K. N. *et al.* Distinct structural and mechanical properties of the nuclear lamina in Hutchinson–Gilford progeria syndrome. *Proc. Natl. Acad. Sci. U S A* **103**, 10271–10276. https://doi.org/10.1073/pnas.0601058103 (2006).
32. Ma, H. *et al.* Multicolor CRISPR labeling of chromosomal loci in human cells. *Proc. Natl. Acad. Sci.* **112**, 3002–3007. https://doi.org/10.1073/pnas.1420024112 (2015).
33. Belton, J. M. *et al.* Hi-C: A comprehensive technique to capture the conformation of genomes. *Methods* **58**, 268–276. https://doi.org/10.1016/j.ymeth.2012.05.001 (2012).
34. Golloshi, R., Sanders, J. T. & McCord, R. P. Iteratively improving Hi-C experiments one step at a time. *Methods* **142**, 47–58. https://doi.org/10.1016/j.ymeth.2018.04.033 (2018).
35. Nagano, T. *et al.* Comparison of Hi-C results using in-solution versus in-nucleus ligation. *Genome Biol* **16**, 175. https://doi.org/10.1186/s13059-015-0753-7 (2015).
36. Imakaev, M. *et al.* Iterative correction of Hi-C data reveals hallmarks of chromosome organization. *Nat. Methods* **9**, 999–1003 (2012).
37. Crane, E. *et al.* Condensin-driven remodelling of X chromosome topology during dosage compensation. *Nature* **523**, 240–244. https://doi.org/10.1038/nature14450 (2015).
38. Rao, S. S. P. *et al.* A 3D map of the human genome at kilobase resolution reveals principles of chromatin looping. *Cell* **159**, 1665–1680. https://doi.org/10.1016/j.cell.2014.11.021 (2014).
39. Kind, J. *et al.* Genome-wide maps of nuclear lamina interactions in single human cells. *Cell* **163**, 134–147. https://doi.org/10.1016/j.cell.2015.08.040 (2015).
40. de Graaf, C., Kind, J., Pagie, L., Peric Hupkes, D. & van Steensel, B. LAD Atlas [Online]. https://osf.io/dk8pm/ (2019).
41. Fudenberg, G. & Mirny, L. A. Higher-order chromatin structure: Bridging physics and biology. *Curr. Opin. Genet. Dev.* **22**, 115–124. https://doi.org/10.1016/j.gde.2012.01.006 (2012).
42. Heinz, S. *et al.* Transcription elongation can affect genome 3D structure. *Cell* **174**, 1522-1536.e1522. https://doi.org/10.1016/j.cell.2018.07.047 (2018).
43. Consortium & E. P,. An integrated encyclopedia of DNA elements in the human genome. *Nature* **489**, 57–74. https://doi.org/10.1038/nature11247 (2012).
44. Liu, Z., Scannell, D. R., Eisen, M. B. & Tjian, R. Control of embryonic stem cell lineage commitment by core promoter factor, TAF3. *Cell* **146**, 720–731. https://doi.org/10.1016/j.cell.2011.08.005 (2011).
45. Bertolino, E. & Singh, H. POU/TBP cooperativity: A mechanism for enhancer action from a distance. *Mol. Cell* **10**, 397–407. https://doi.org/10.1016/S1097-2765(02)00597-X (2002).
46. Krietenstein, N. *et al.* Ultrastructural details of mammalian chromosome architecture. *Mol. Cell* **78**, 554-565.e557. https://doi.org/10.1016/j.molcel.2020.03.003 (2020).
47. Wang, Z. *et al.* Genome-wide mapping of HATs and HDACs reveals distinct functions in active and inactive genes. *Cell* **138**, 1019–1031. https://doi.org/10.1016/j.cell.2009.06.049 (2009).
48. Bustos, M. A. *et al.* Genome-wide chromatin accessibility, DNA methylation and gene expression analysis of histone deacetylase inhibition in triple-negative breast cancer. *Genom Data* **12**, 14–16. https://doi.org/10.1016/j.gdata.2017.01.002 (2017).
49. Stephens, A. D. *et al.* Chromatin histone modifications and rigidity affect nuclear morphology independent of lamins. *Mol. Biol. Cell* **29**, 220–233. https://doi.org/10.1091/mbc.E17-06-0410 (2018).
50. Sardo, L. *et al.* Real-time visualization of chromatin modification in isolated nuclei. *J. Cell Sci.* **130**, 2926–2940. https://doi.org/10.1242/jcs.205823 (2017).
51. Florescu, A.-M., Therizols, P. & Rosa, A. Large scale chromosome folding is stable against local changes in chromatin structure. *PLoS Comput. Biol.* **12**, e1004987. https://doi.org/10.1371/journal.pcbi.1004987 (2016).
52. Stephens, A. D., Banigan, E. J., Adam, S. A., Goldman, R. D. & Marko, J. F. Chromatin and lamin A determine two different mechanical response regimes of the cell nucleus. *Mol. Biol. Cell* https://doi.org/10.1091/mbc.E16-09-0653 (2017).
53. Golloshi, R. *et al.* Constricted migration is associated with stable 3D genome structure differences in melanoma cells. *bioRxiv* https://doi.org/10.1101/856583 (2020).
54. Jacobson, E. C. *et al.* Migration through a small pore disrupts inactive chromatin organization in neutrophil-like cells. *BMC Biol.* **16**, 142. https://doi.org/10.1186/s12915-018-0608-2 (2018).
55. Visvanathan, A. *et al.* Modulation of higher order chromatin conformation in mammalian cell nuclei can be mediated by polyamines and divalent cations. *PLoS ONE* **8**, e67689. https://doi.org/10.1371/journal.pone.0067689 (2013).
56. Kirmes, I. *et al.* A transient ischemic environment induces reversible compaction of chromatin. *Genome Biol.* **16**, 246–246. https://doi.org/10.1186/s13059-015-0802-2 (2015).
57. Lindsay, R. J., Pham, B., Shen, T. & McCord, R. P. Characterizing the 3D structure and dynamics of chromosomes and proteins in a common contact matrix framework. *Nucleic Acids Res.* https://doi.org/10.1093/nar/gky604 (2018).
58. Liu, Y. & Dekker, J. Biochemically distinct cohesin complexes mediate positioned loops between CTCF sites and dynamic loops within chromatin domains. *bioRxiv* https://doi.org/10.1101/2021.08.24.457555 (2021).
59. Balajee, A. S. *et al.* Investigation of spatial organization of chromosome territories in chromosome exchange aberrations after ionizing radiation exposure. *Health Phys.* **115**, 77–89. https://doi.org/10.1097/HP.0000000000000840 (2018).
60. Sanders, J. T. *et al.* Radiation-induced DNA damage and repair effects on 3D genome organization. *Nat. Commun.* **11**, 6178. https://doi.org/10.1038/s41467-020-20047-w (2020).
61. Zhang, Y. *et al.* Spatial organization of the mouse genome and its role in recurrent chromosomal translocations. *Cell* **148**, 908–921. https://doi.org/10.1016/j.cell.2012.02.002 (2012).
62. Ramírez, F. *et al.* deepTools2: A next generation web server for deep-sequencing data analysis. *Nucleic Acids Res.* **44**, W160–W165. https://doi.org/10.1093/nar/gkw257 (2016).
63. Quinlan, A. R. & Hall, I. M. BEDTools: A flexible suite of utilities for comparing genomic features. *Bioinformatics* **26**, 841–842. https://doi.org/10.1093/bioinformatics/btq033 (2010).

Acknowledgements
We thank Sarah Carver, Trevor Freeman, Jansi Srinivasan, and Jeff Schoondyke for assistance with some expansion experiments and quantification, and Houda Belaghzal for advice on digestion conditions. We thank Justin Lindsay for assistance with computational analysis, Bryan Lajoie, Hakan Ozadam, and Junwen Li for assistance with computational pipelines, and Noam Kaplan for helpful conversations. We thank Adayabalam Balajee for assistance with mFISH chromosome territory imaging. This work was supported in part by NIH NIGMS Grants F32GM100617 and R35GM133557 to R.P.M., and NIH Grant HG003143 to J.D. J.D. is an investigator of the Howard Hughes Medical Institute.

Author contributions
J.T.S. and R.G. performed Hi-C and imaging experiments, analyzed data, and contributed to writing the manuscript. P.D. performed ridge and random forest regression modeling and compartment strength analyses. Y.X. performed aggregate insulation score analyses. P.H.T. performed and analyzed digestion and CRISPR imaging experiments and contributed to writing the manuscript. D.N. performed and analyzed digestion expansion experiments. J.D. provided advice for designing the study and performing experiments, analyses, and writing the manuscript. R.P.M. conceived the study, performed Hi-C and imaging experiments, analyzed data, and wrote the manuscript.

Competing interests
The authors declare no competing interests.

Additional information
Supplementary Information The online version contains supplementary material available at https://doi.org/10.1038/s41598-022-08602-5.

Correspondence and requests for materials should be addressed to R.P.M.

Reprints and permissions information is available at www.nature.com/reprints.

Publisher's note Springer Nature remains neutral with regard to jurisdictional claims in published maps and institutional affiliations.